Phase shift of polarized light through sculptured thin films: Experimental measurements and theoretical study*

Hou Yong-Qiang(侯永强)[a)b)], Qi Hong-Ji(齐红基)[a)†], Li Xu(李 煦)[a)], He Kai(何 凯)[a)], Yi Kui(易 葵)[a)], and Shao Jian-Da(邵建达)[a)]

[a)] *Key Laboratory of Materials for High Power Laser, Shanghai Institute of Optics and Fine Mechanics, Chinese Academy of Sciences, Shanghai* 201800, *China*

[b)] *Shanghai Huali Microelectronics Corporation, Shanghai* 201203, *China*

(Received 21 March 2013; revised manuscript received 8 May 2013)

A slanted columnar TiO_2 sculptured anisotropic thin film (ATF) is prepared via the glancing angle deposition technique and used as the phase retardation plate. The tilted nanocolumn microstructures of thin film induce the optical anisotropy. With the biaxial birefringent model, the optical constants dispersion equations of TiO_2 ATF are derived by fitting the transmittance spectra for s- and p-polarized waves measured at normal and oblique incidence within 400 nm–1200 nm. The phase shift of polarized light after reflection and/or transmission through the TiO_2 ATF is analyzed with the characteristic matrix employing the extracted structure parameters. The theoretical studies reasonably well accord with the experimental results measured with spectroscopic ellipsometry. In addition, the dependences of the phase shift on the coating physical thickness and oblique incidence angle are also discussed. Birefringence of the biaxial ATF provides a sophisticated phase modulation by varying incidence angles over a broad range to have a wide-angle phase shift.

Keywords: birefringence, thin films, optical properties, phase shift

PACS: 78.20.Fm, 78.20.Ci, 42.25.Ja **DOI:** 10.1088/1674-1056/22/12/127801

1. Introduction

Three-dimensional (3D) nanoengineered anisotropic sculptured thin film (STF)[1–3] prepared via the glancing angle deposition (GLAD) technique resembles an artificial material with interesting optical properties and is extensively adopted in designing and developing optical components, including phase retardation devices,[4–8] polarization-selective beam splitters,[9] polarization converters and interferometer,[10,11] broadband antireflective coatings,[12–14] rugate and grating filters,[15–17] etc. On the other hand, such films deposited in a controllable manner during growth show that the nanocolumn microstructures exhibit continuum and anisotropic characteristics, but the molecules and clusters of small size retain their individuality. In addition, the densities of these films are significantly lower than those of bulk counterparts due to the self-shadowing and surface diffusion effects in obliquely deposited thin films. As a consequence, the STFs can also meet the requirements of a variety of applications such as catalytic surfaces,[18] micro-sensor elements,[19–21] and 3D photonic crystals[22,23] by virtue of their high porosity, periodicity, and chirality. In contrast to conventional optical phase retarders that are constructed from birefringent crystals, such as quartz waveplate, etc., devices designed with ATFs can perform better in manipulating the polarization state of electromagnetic waves because the ATF presents birefringence. This property is very important for the polarization and phase components for the miniaturization of integrated optical systems.

In the research described in this paper, because of a large bulk refractive index ($n_{TiO_2} = 2.6$), good mechanical and thermal stability, high static dielectric constant, and excellent transparency at UV/VIS/NIR wavelengths, the sculptured titanium dioxide ATF with a highly orientated microstructure composed of slanted nanocolumns is prepared, and the optical properties, including three principal indices, column angle, and phase shift of polarized light after reflection and/or transmission through the ATF are characterized with polarization transmittance spectra, spectroscopic ellipsometry[24–27] and scanning electron microscopy. The results demonstrate that the polarization state of electromagnetic waves and phase shift can be modulated by selecting the appropriate birefringence and coating thickness of ATF. Birefringence of the biaxial ATF provides a sophisticated phase modulation by varying incidence angles over a broad range to have a wide-angle phase shift.

2. Fundamental theory: phase shift of polarized light after reflection and/or transmission through biaxial anisotropic thin films

For isotropic layers of thin films, the calculation of the phase shift for two polarized states and the influence of the sample azimuth on phase shift are well known. By comparison with isotropic thin films, the treatment of the ATFs is

*Project supported by the National Natural Science Foundation of China (Grant No. 61205211).

†Corresponding author. E-mail: qhj@mail.siom.ac.cn

© 2013 Chinese Physical Society and IOP Publishing Ltd

mathematically quite complicated. Even with 4×4 transmission matrices, the characteristic parameters such as the directions of wave vectors and rays, as well as the angles of refraction, could not be clearly described when the wave propagates across and through the ATF in a general way. At the same time, the tilted columnar ATF deposited with GLAD technique is generally biaxial, where one of the principal axes (labeled 1) is oriented in the direction of the columns, while the other principal axis (labeled 2) is perpendicular to the principal axis 1 and located in the deposition plane. Another principal axis (labeled 3) is perpendicular to the plane of deposition as shown in Fig. 1. The incident medium and substrate are homogeneous and isotropic media, and n_0 and n_g are the corresponding refractive indices. The plane wave is incident from the incident medium at an angle θ_0 and yields the refractive angle θ_g in the substrate. Thus, the optical properties of a biaxial film are determined by the three principal refractive indices n_1, n_2, and n_3, column angle β, and coating physical thickness d. Without loss of generality, we consider the deposition plane of biaxial ATF to be consistent with the plane of incidence, that is to say, the principal section coincides with the principal plane. In this case, the propagations of TE and TM waves are decoupled and the 4×4 matrix breaks up into two 2×2 matrixes. The TE wave propagates in an ordinary manner independent of the propagation direction. By contrast, the TM wave propagates in an extraordinary manner. The forward- and backward-propagating directions of wave vectors generally differ from those of rays in birefringent thin film, that is to say, the propagating directions of rays and wave vectors are not identical. Under the boundary continuity condition of Maxwell's equations, our previous study[28–30] has deduced the 2×2 characteristic matrices for the ordinary and extraordinary waves and they are represented below.

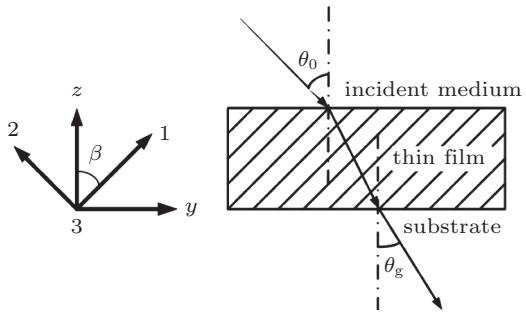


Fig. 1. Schematic diagram of a biaxial ATF model.

For an s-polarized wave, the optical properties are equivalent to those of isotropic thin film and determined by the refractive index n_3, refraction angle θ_s, and physical thickness d of the biaxial film, and can be described with the characteristic matrix $\begin{bmatrix} \cos\delta_s & (\mathrm{i}/\eta_s)\sin\delta_s \\ \mathrm{i}\eta_s\sin\delta_s & \cos\delta_s \end{bmatrix}$, where $\eta_s = n_3\cos(\theta_s)$, $\delta_s = (2\pi/\lambda)n_3 d\cos(\theta_s)$, with η_s and δ_s defined as the effective optical admittance and phase thickness, respectively.

For p-polarized wave, the differences in refractive index between forward- and backward-propagating directions of wave vectors

$$n(\alpha_1) = \frac{1}{(\sin^2\alpha_1/n_2^2 + \cos^2\alpha_1/n_1^2)^{1/2}}$$

and

$$n(\alpha_2) = \frac{1}{(\sin^2\alpha_2/n_2^2 + \cos^2\alpha_2/n_1^2)^{1/2}},$$

lead to different values of phase thickness $\delta_+ = (2\pi/\lambda)n(\alpha_1)d\cos\theta_1$ and $\delta_- = (2\pi/\lambda)n(\alpha_2)d\cos\theta_2$. The effective optical admittances of forward- and backward-traveling waves are determined by the directions of rays, and given by $\eta_+ = n(\beta_1)/\cos\xi_1$ and $\eta_- = n(\beta_2)/\cos\xi_2$, respectively. On the basis of the above theoretical derivations, the 2×2 characteristic matrix can be described by

$$\frac{1}{\eta_+ + \eta_-}\begin{bmatrix} \eta_- \mathrm{e}^{\mathrm{i}\delta_+} + \eta_+ \mathrm{e}^{-\mathrm{i}\delta_-} & \mathrm{e}^{\mathrm{i}\delta_+} - \mathrm{e}^{-\mathrm{i}\delta_-} \\ \eta_-\eta_+(\mathrm{e}^{\mathrm{i}\delta_+} - \mathrm{e}^{-\mathrm{i}\delta_-}) & \eta_+ \mathrm{e}^{\mathrm{i}\delta_+} + \eta_- \mathrm{e}^{-\mathrm{i}\delta_-} \end{bmatrix}.$$

The characteristic matrix of the assembly can be given by $\begin{bmatrix} B \\ C \end{bmatrix} = M \cdot \begin{bmatrix} 1 \\ \eta_g \end{bmatrix}$, where M is the combined characteristic matrix of the thin film for ordinary and/or extraordinary wave, B and C are the normalized electric and magnetic fields at the front interface and can be used to extract the optical properties of the biaxial ATF. The input optical admittance of the assembly Y is defined as $Y = C/B$. This result can be immediately extended to the general case of an assembly of n anisotropic layers with the principal section coincident with the principal plane. The characteristic matrix of the assembly is simply the product of the individual matrices taken in the correct order and shown as

$$\begin{bmatrix} B \\ C \end{bmatrix} = M_n M_{n-1} \cdots M_2 M_1 \begin{bmatrix} B \\ C \end{bmatrix} = M \cdot \begin{bmatrix} 1 \\ \eta_g \end{bmatrix},$$

where M_n is the characteristic matrix of the n-th layer and different for two polarizations.

Just for the isotropic thin film, the matrix relationship given above and Fresnel's law lead to the phase shift on reflection φ and transmission ξ of the assembly as follows:[31]

$$\varphi = \arctan\left\{\frac{\mathrm{Im}[\eta_0(BC^* - CB^*)]}{\eta_0^2 BB^* - CC^*}\right\}, \quad (1)$$

$$\xi = \arctan\left[\frac{-\mathrm{Im}(\eta_0 B + C)}{\mathrm{Re}(\eta_0 B + C)}\right], \quad (2)$$

where η_0 is the incident medium effective optical admittance and $\eta_0 = n_0\cos\theta_0$ for s-polarized wave and $\eta_0 = n_0/\cos\theta_0$ for p-polarized wave.

3. Experiments: preparation and characterization of the TiO_2 biaxial anisotropic sculptured thin film

The TiO_2 biaxial ATF was deposited onto flat fused silica (Φ30 mm $\times$ 3 mm) substrate through reactive-electron beam evaporation in a laboratory high vacuum deposition system configured for the GLAD technique. In this method the physical vapor deposition is used to deposit films on a substrate that is tilted at a deposition angle with respect to the vapor source as shown schematically in Fig. 2. The tilting and rotating of the substrate were automatically controlled with two step motors so that the void region between the nanocolumns and the volume fraction of the deposited STF can also be controlled with this process. An INFICON IC/5 quartz crystal monitor was located near the substrate and used to measure the deposition rate and thickness of the growing film. A well-controlled deposition rate resulted in a uniform pitch. In our experiment, the substrate was ultrasonically cleaned in acetone and ethanol before being introduced into the vacuum system. The deposition angle α that refers to the angle between the substrate normal and the impinging direction of the vapor flux, was fixed to be 70°. During the deposition, the substrate was maintained at room temperature and no rotation was introduced. The chamber base pressure was pumped to less than 2.0×10^{-3} Pa. To keep the stoichiometry of the TiO_2 ATF, ultrahigh purity O_2 (99.99%) was incorporated to obtain a background pressure of 2.7×10^{-2} Pa during the growth of the thin film.

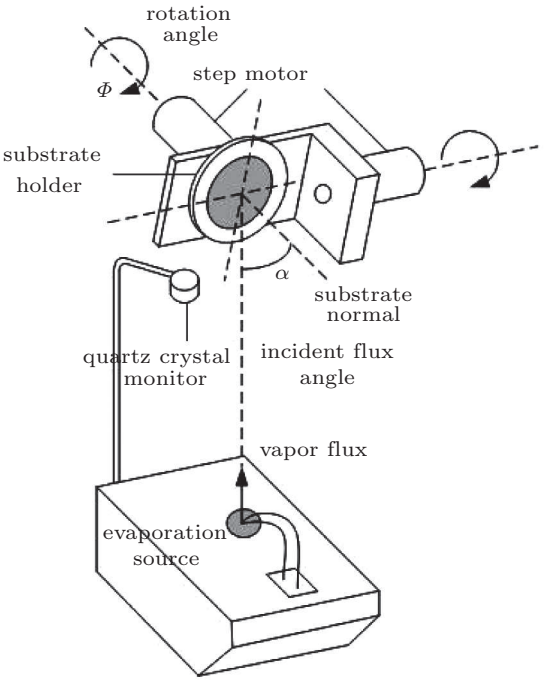


Fig. 2. Schematic diagram of the GLAD process.

The cross-sectional morphology of the TiO_2 ATF was observed by scanning electron microscopy (SEM) using a Zeiss Auriga Crossbeam microscope. For better preparation of SEM observation, the ATF was coated with a thin layer of n-Si (100) to improve conduction. To experimentally investigate the phase shift of polarized light after reflection and/or transmission through sculptured ATF, spectroscopic ellipsometry measurements were performed in the deposition plane by varying incidence angles using a Horiba Scientific system in a laboratory environment.

Polarization transmittance measurements of the TiO_2 ATF were performed in air and a wavelength range from 400 nm to 1200 nm with a Perkin–Elmer UV/VIS/NIR Lambda 1050 spectrophotometry. The schematic diagram of the measurement device is shown in Fig. 3. The polarizer was introduced to obtain two orthogonal directions of the polarization wave. In our measurements, an integrated sphere was used in the detector and a blank fused silica substrate was inserted between the sample and detector to eliminate the effect of beam shift at oblique incidence. The position of the sample was carefully adjusted so that the incident plane was coincident with the deposition plane when measured at different incidence angles. In addition, the raw data were dealt to eliminate the back reflection of substrate after measurement according to the formula $T_f = (1 - R_G)/(T_G/T - R_G)$, where T, T_G, and R_G represent the raw transmittance of the sample, the transmittance, and reflectance of air-substrate interface, respectively.

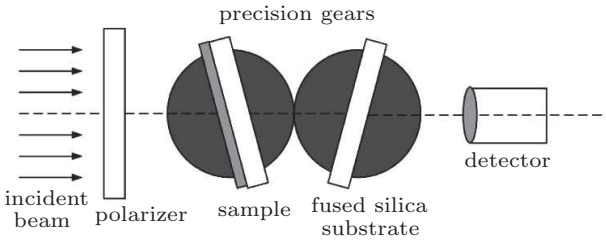


Fig. 3. Schematic diagram of the polarization transmittance measurement device.

4. Results and discussion

4.1. Microstructure of the TiO_2 ATF

The cross sectional SEM image is shown in Fig. 4. The section of the deposited TiO_2 biaxial ATF is coincident with the deposition plane, defined as the direction of column growth with respect to the substrate normal. As can be seen, the typical sculptured microstructures with highly orientated tilted nanocolumns are exhibited and tended to become the optical anisotropic permittivity of the thin film. Furthermore, owing to the self-shadowing and surface diffusion effects, the film grows with a highly porous columnar structure that is slanted toward the vapor flux. Pores between columns are a significant characteristic of GLAD-produced films and the porous structure will inevitably influence the phase shift of ATF. The

thickness and oblique angle of the nanocolumns are measured to be about 985.63 nm and 39.8°, respectively.

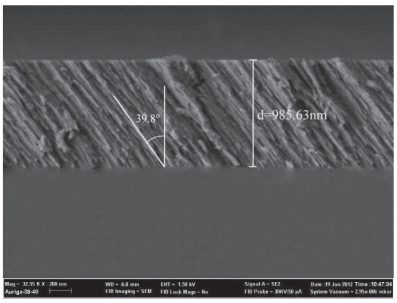


Fig. 4. Cross-sectional SEM image of the TiO_2 ATF deposited at $\alpha = 70°$.

4.2. Phase shift of polarized light through the TiO_2 ATF

The transmittance spectra of the ATF, measured at normal and oblique incidences of 15°, 30°, and 45° for two polarized states, are plotted in Figs. 5(a) and 5(b). As shown in Fig. 5, the transmittance spectra appear as obvious interference modulations caused by multiple reflections at film interfaces and separate at normal incidence for TE and TM waves, indicating that our prepared TiO_2 ATF with highly orientated microstructure composed of slanted nanocolumns is optically anisotropic. With the increase of incidence angle, the spectra shift toward shorter wavelengths (blue-shift) for two polarizations. Furthermore, the peak-valley values of interference fringes are enhanced for TE waves, but weakened for TM waves.

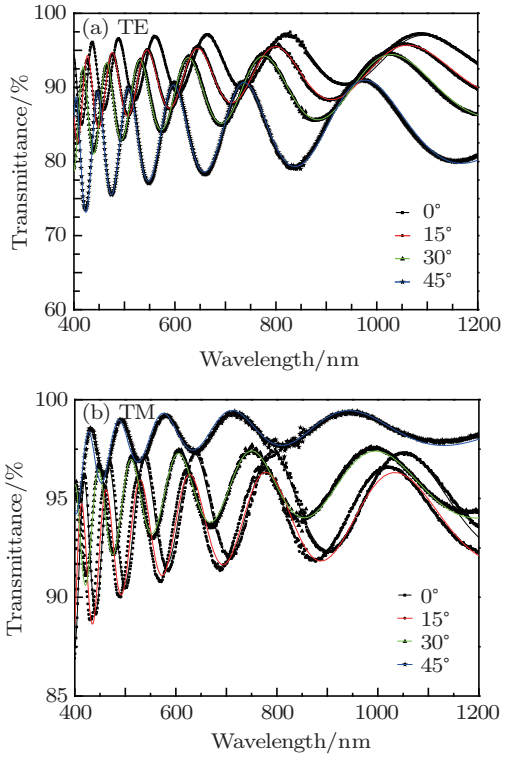


Fig. 5. (color online) Transmittance spectra of the as-deposited TiO_2 ATF with different incidence angles for (a) TE and (b) TM waves.

The extraction of optical constants for the biaxial ATF using multiwavelength curve fitting methods is similar to that in our previous work.[32] The dispersion equations are derived by fitting the transmittance spectra for s- and p-polarized waves within 400 nm–1200 nm using an inverse synthesis method, and by gradually adjusting the initial values of the coefficients of dispersion equations until a better optimization is achieved between the experimental measurements and theoretical results. Based on the Cauchy model, the dispersion of principle refractive indices and the extinction coefficient for TE and TM waves are exhibited in Figs. 6(a) and 6(b). The optimization gives the physical thickness $d = 992.552$ nm and column angle $\beta = 39.36°$, which well accord with those obtained from the SEM image. Employing the extracted optical constants and physical thickness, the transmittance fitting curves for two polarized state waves are inversely calculated and the results are also shown in Figs. 5(a) and 5(b). The fitting transmittance curves clearly coincide with the measured spectra.

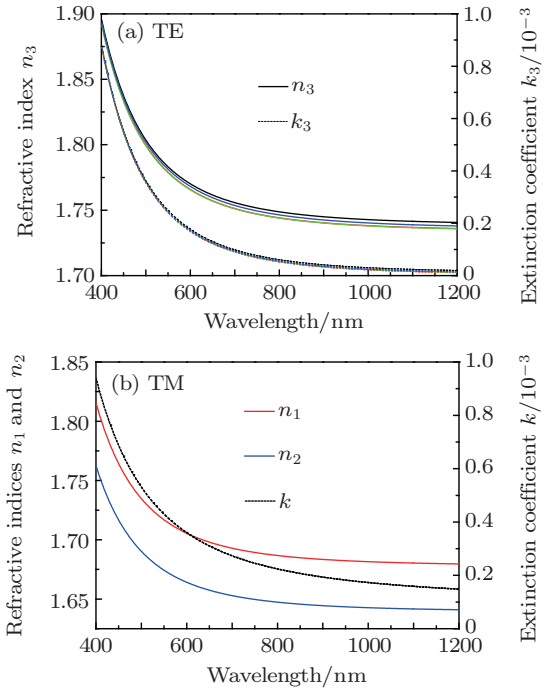


Fig. 6. (color online) Dispersion curves of principle refractive index and extinction coefficient determined with the transmittance spectra of the TiO_2 ATF for (a) TE and (b) TM waves.

With the above-mentioned structure parameters $n_1 = 1.70$, $n_2 = 1.66$, $n_3 = 1.762$, $\beta = 39.36°$, and $d = 992.552$ nm of the TiO_2 ATF at a wavelength of $\lambda = 632.8$ nm, the phase shift spectra of polarized light after reflection at 45° oblique incidence and/or transmission at normal incidence are analyzed with characteristic matrix by considering the interference effects of thin films, which are shown in Figs. 7(a) and 7(b), respectively. The effective refractive index of the extraordinary wave propagating in the ATF is

$$n_p = \frac{1}{(\sin^2\beta/n_1^2 + \cos^2\beta/n_2^2)^{1/2}} = 1.6836$$

at normal incidence and the birefringent property $\Delta n = n_s - n_p = 0.0784$. For the method of calculating the conventional simplified phase shift, considering the fact that its essence is based on the waveplates design of quartz crystal in bulk, this method is only valid at normal incidence for phase shift on transmission and $\Delta\varphi$ is simply assumed to be proportional to the birefringence Δn and thickness d satisfies the formula $\Delta\varphi = 2\pi(n_s - n_p)d/\lambda$. For better comparison, the experimentally measured phase shift spectra in the deposition plane are also shown in the same plot.

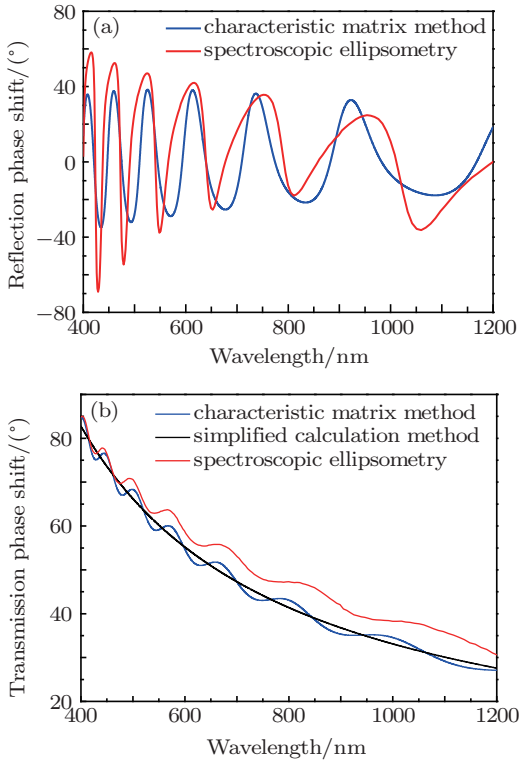


Fig. 7. (color online) Phase shift spectra of polarized light through the TiO_2 ATF: (a) reflection phase shift at 45° oblique incidence and (b) transmission phase shift at normal incidence.

4.3. Angular performance

The phase shift of polarized light after reflection and/or transmission through the ATF can be easily analyzed using the characteristic matrix method for the case of oblique incidence, by comparison of using the simplified calculation method. Figure 8 illustrates the dependences of phase shift on oblique incidence angle. As can be seen, both reflection and transmission phase shifts are continuously adjustable by increasing incidence angle. Moreover, the phase shift shows an asymmetrical angular-selective performance for the light incident at the same positive and negative incidence angle, even though the profiles of the reflection phase shift seem to be symmetrical. The experimental spectroscopic ellipsometry measurements at different symmetrical incidence angles verify the theoretical analyzed results. Birefringence of the ATF provides a sophisticated phase modulation by varying incidence angle over a broad range to have a wide-angle phase shift.

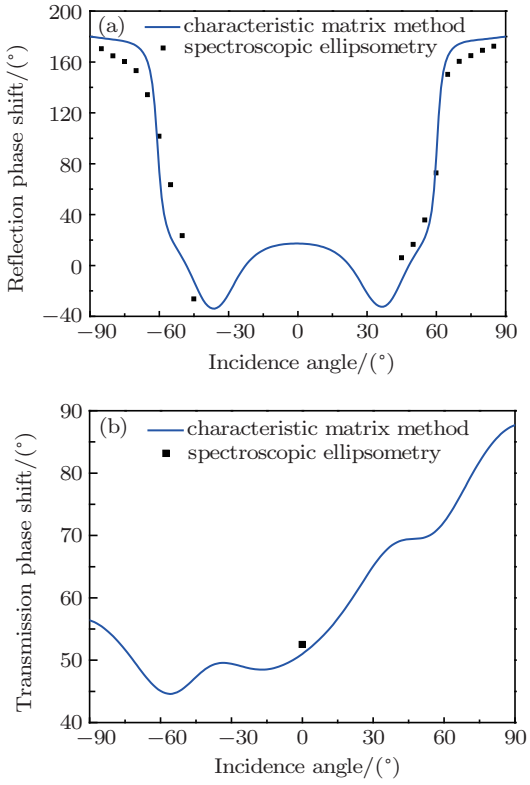


Fig. 8. (color online) Dependences of phase shift on oblique incidence angle: (a) reflection phase shift and (b) transmission phase shift.

4.4. Effect of physical thickness on the phase shift of polarized light through the ATF

Considering the limitations of our experimental conditions, we cannot *in situ* study the influence of physical thickness on the phase shift of polarized light through ATF. Accordingly, we theoretically investigate the relationships between the coating physical thickness and the phase shift of polarized light after reflection at 45° oblique incidence and/or transmission at normal incidence with the characteristic matrix, and plot them in Figs. 9(a) and 9(b), respectively. As shown in Fig. 9, both reflection and transmission phase shifts clearly exhibit modulations caused by the interference effects of thin film. It should be noted that with the increase of thickness, the envelope of peak-valley values of exact phase shift interference fringes are also modulated, which may be attributed to the complicated nonlinear relationships between the optical phase shift and coating thickness.[33] For a better illustration, the transmission phase shift is dealt with by eliminating the linear phase shift and, it is shown in the same plot (Fig. 9(b)).

In summary, we investigate the phase shifts of polarized light after reflection and/or transmission through TiO_2 ATF and demonstrated the feasibility of achieving a wide-angle phase retardation plate by using an ATF. A reasonably good agreement is observed but some slight deviations and drifts still exist between the theoretical results analyzed with the characteristic matrix and experimental results measured in the deposition plane by spectroscopic ellipsometry as seen in Figs. 7 and 8. This finding is mainly attributed to the idealized optical model, nanostructure confinement effects, and

the inherent large surface-to-volume ratio, which can affect the polarization of the ATF. Moreover, the non-uniformity of our prepared tilted columnar ATF is caused by the self-shadowing effect and limited mobility of the deposited atoms, the difference in ambient humidity level and temperature range in the two test environments between the spectrophotometry and spectroscopic ellipsometry measurements may also lead to the changes. However, the phase shift of the ATF produced by non-uniformity is very sensitive to the incidence angle, wavelength, and polarization. In addition, TiO_2 demonstrates the photocatalytic self-cleaning phenomenon: ultraviolet illumination of TiO_2 generates electron-hole pairs that react with organic contaminants on the surface to produce several compounds including CO_2 and H_2O and desorption from surface.[34] This self-cleaning effect might have an influence on the phase shift sensitivity. The effect of water–vapor adsorption on the phase shift must be investigated and quantified in a controlled environment in our further research.

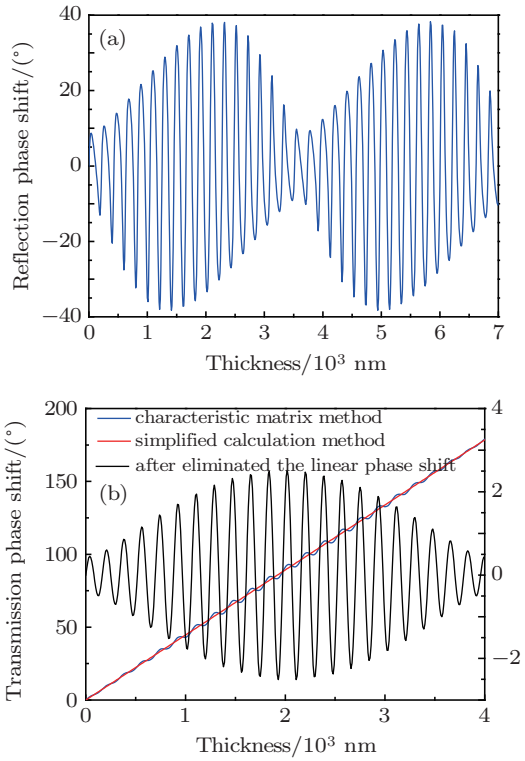


Fig. 9. (color online) Influence of the coating physical thickness of the TiO_2 ATF on the phase shift: (a) reflection phase shift at 45° oblique incidence and (b) transmission phase shift at normal incidence.

5. Conclusions

In this article, the sculptured TiO_2 ATF is successfully prepared by reactive electron-beam evaporation via GLAD technique. The ATF exhibits a highly orientated microstructure composed of slanted nanocolumns. The birefringence is ascribed to the orientated growth and anisotropic microstructure of the thin film. The phase shifts of polarized light after reflection and/or transmission through the TiO_2 ATF are analyzed with the characteristic matrix method. The theoretical studies of phase shift reasonably well accord with the experimental results, thereby validating the model established for this kind of GLAD-produced film, the greater generality, and superiority of characteristic matrix. This work demonstrates that the polarization state of the electromagnetic wave and phase shift can be modulated by using an ATF. The birefringence of the ATF provides a sophisticated phase modulation by varying incidence angle over a broad range to have a wide-angle phase shift. We make an encouraging attempt at designing a phase retardation plate using ATF and anticipate that the phase shift obtained with this method will permit the initiation of designing more flexible optical components in a range of biaxial anisotropic coatings.

References

[1] Robbie K, Brett M J and Lakhtakia A 1996 *Nature* **384** 616
[2] Wang J G, Shao J D, Wang S M, He H B and Fan Z X 2005 *Chin. Phys. Lett.* **22** 2066
[3] Wang J G, Shao J D and Fan Z X 2005 *Chin. Phys. Lett.* **22** 221
[4] Motohiro T and Taga Y 1989 *Appl. Opt.* **28** 2466
[5] Hodgkinson I, Wu Q H, De Silva L and Arnold M 2004 *Opt. Express* **12** 3840
[6] Wei Z H, Wang R, Pu T, Sun G D and Fang T 2013 *Chin. Opt. Lett.* **11** S20601
[7] Zhou H, Qiu K and Tian F F 2012 *Chin. Opt. Lett.* **10** 050601
[8] Wen H, Liao J X, Zheng X P, Zhang H Y and Guo Y L 2012 *Chin. Opt. Lett.* **10** 070601
[9] Qi H J, Hong R J, Yi K, Shao J D and Fan Z X 2005 *Appl. Opt.* **44** 2343
[10] Lin C F and Jen Y J 2012 *J. Nanophotonics* **6** 061507
[11] Zhu L L, Zeng A J, Li F Y and Huang H J 2012 *Chin. Opt. Lett.* **10** 061201
[12] Xi J Q, Schubert M F, Kim J K, Schubert E F, Chen M F, Lin S Y, Liu W and Smart J A 2007 *Nat. Photon.* **1** 176
[13] Zhang J C, Fang M, Jin Y X and He H B 2012 *Chin. Phys. B* **21** 014202
[14] Guo T T, Zheng L Q, Nshimiyimana J P, Diao X G and Chen Q 2013 *Chin. Opt. Lett.* **11** S10103
[15] Zhang J C, Fang M, Shao Y C, Jin Y X and He H B 2011 *Chin. Phys. B* **20** 094212
[16] Zhang J C, Fang M, Shao Y C, Jin Y X and He H B 2012 *Chin. Phys. B* **21** 054219
[17] Shi Y J and Gu Z T 2012 *Chin. Opt. Lett.* **10** 080602
[18] Gibbs J G and Zhao Y P 2009 *Small* **5** 2304
[19] Lahktakia A 1998 *Sens. Actuators B: Chem.* **52** 243
[20] Liu Y J, Shi J J, Zhang F, Liang H N, Xu J, Lakhtakia A, Fonash S J and HuangT J 2011 *Sens. Actuators B: Chem.* **156** 593
[21] Shalabney Atef, Khare C, Rauschenbach B and Abdulhalim I 2011 *Sens. Actuators B: Chem.* **159** 201
[22] Venugopal V C 2012 *Proceedings of Nanostructured Thin Films V*, ed. Mackay T G, Jen Y J and Martin-Palma (San Diego: SPIE)
[23] Lou S Q, Wang Z, Ren G B and Jian S S 2004 *Chin. Phys.* **13** 1493
[24] Hodgkinson I, Hazel J C and Wu Q H 1998 *Thin Solid Films* **313–314** 368
[25] Franke E, Schubert M, Trimble C L, DeVries M J and Woollam J A 2001 *Thin Solid Films* **388** 283
[26] Schmidt D, Booso B, Hofmann T, Schubert E, Sarangan A and Schubert M 2009 *Appl. Phys. Lett.* **94** 011914
[27] Schmidt D, Booso B, Hofmann T, Schubert E, Sarangan A and Schubert M 2009 *Opt. Lett.* **34** 992
[28] Qi H J, Zhang D P, Shao J D and Fan Z X 2005 *Europhys. Lett.* **70** 257
[29] Qi H J, Shao J D and Fan Z X 2007 *Europhys. Lett.* **78** 17004
[30] Hou Y Q, Li X, He K, Qi H J, Yi K and Shao J D 2013 *Chin. Phys. Lett.* **30** 017802
[31] Macleod H A 2010 *Thin-Film Optical Filters*, 4th edn. (Boca Rotan: CRC) pp. 13–57
[32] Qi H J, Xiao X D, He H B, Yi K and Fan Z X 2009 *Appl. Opt.* **48** 127
[33] Qi H J, Zhu M P, Zhang W L, Yi K, He H B and Shao J D 2012 *Chin. Opt. Lett.* **10** 013104
[34] Taschuk M T, Steele J J, van Popta A C and Brett M J 2008 *Sens. Actuators B: Chem.* **134** 666